Rotational Detonation Engine for Hypersonic Flight

Mr. Michael Paluszek[*,a], Dr. Christopher Galea[a], Mr. Miles Simpkins[b], Dr. Yiguang Ju[b], and Dr. Mikhail Shneider[b]

[a]*Princeton Satellite Systems, Plainsboro, NJ*
[b]*Princeton University, Princeton, NJ*
[*]Corresponding author

ABSTRACT

Hypersonic aircraft and missiles are of great interest. Potential applications include military reconnaissance and strike, passenger aircraft, and the first stage for a two-stage to orbit launch vehicle. Numerous engines have been proposed for hypersonic vehicles including a wide variety of combined cycle engines, including those with integrated rockets and scramjets. This paper presents the analysis, design, and simulation of a Rotating Detonation Engine (RDE) powered test vehicle that can reach high Mach numbers. The paper covers the analysis of the engine with analytical studies. The aircraft, the size of a hobbyist jet aircraft, that would be used to verify the flight performance of the engine is then presented. Non-linear dynamic inversion techniques are used to design a guidance law. End-to-end simulations, including verification of the aircraft's overall flight phases, are presented. Finally, the development plan for a cruise missile-sized test vehicle is discussed.

1. INTRODUCTION

Hypersonic aircraft and missiles are of great interest. Potential applications include military reconnaissance and strike, passenger aircraft and the first stage for a two-stage to orbit launch vehicle [1, 2, 3, 4, 5]. Numerous engines have been proposed for hypersonic vehicles including a wide variety of combined cycle engines, including those with integrated rockets and scramjets. Engines that have been tested or are currently under test include the Sänger II turboramjet [6] and the Reaction Engines Limited [7] cooled inlet engine.

Our specific application is an engine for a two-stage to orbit launch vehicle. The first stage takes off from an airfield and accelerates to a high Mach number and then the second stage separates. The second stage uses an LH_2/LO_2 engine, such as the Aerojet Rocketdyne's RL-10 to take the spacecraft into orbit and return the second stage to the airfield. The first stage returns to the launch site at subsonic speeds. The first stage engine is the subject of this paper. The entire two-stage to orbit vehicle is discussed in detail in [1].

The turbopump allows operation up to Mach 1.25 and is capable of accelerating through Mach 1. An important point to note is that the ramjet is only used as an accelerator. This greatly decreases the stress on the engine compared to one that must operate for hours at high Mach cruise speeds. Coaxial ramjets are not new. The J58 engine in the SR-71 was a coaxial ramjet designed to cruise at Mach 3.2. The coaxial ramjet is the same concept that was proposed for the Sänger two stage to orbit vehicle [8]. The engine is shown in the test in Figure 1.

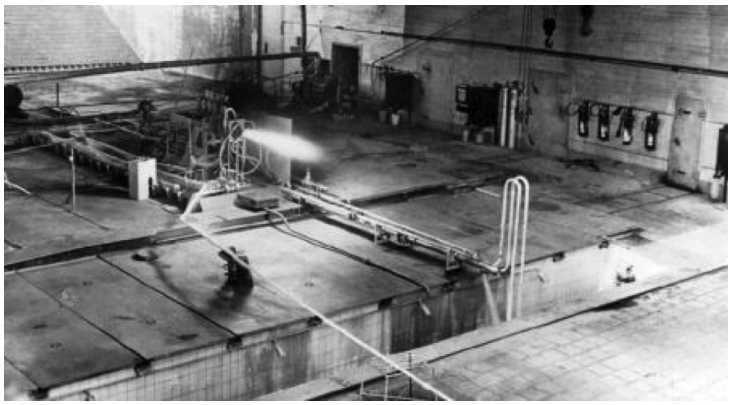

Figure 1: The hydrogen-fueled MBB Turboramjet in test [9]. The Sänger first stage would cruise at Mach 4 and accelerate to Mach 6.8 before second stage separation.

Figure 2 on the next page shows the thrust and specific impulse as a function of Mach number over a trajectory varying linearly with Mach number from 0 to 40 km. The transition from turbopump to ramjet is Mach 1.25. Analytical models are used for both modes.

Figure 3 on the facing page shows a typical ascent. In this case, separation is at Mach 5.6. The endpoint is sufficient for the use of a single upper stage.

The RDE has the potential to improve combustor efficiency. Recent work on RDEs includes an in-space flight test [10, 11] as well as laboratory experimental and computational studies [12, 13]. It may be possible to reach Mach numbers above 6.8, the number planned for the Sänger.

This paper studies an engine with a Rotating Detonation Engine combustor and a turbopump at the inlet to drive the RDE combustor until ram pressure is sufficient. We present an analytical model of the engine. We then present a Radio Controlled aircraft design for flight testing of the RDE. This aircraft is the size of commercially available radio-controlled model jet aircraft but with the capability to reach supersonic speeds to test the turbopump to ram transition. The aircraft is designed for short-duration flights. The range is limited by the volume of hydrogen fuel it can carry. The control system design is presented.

The aircraft design discussion is followed by end-to-end simulations of the aircraft. Control of the aircraft during all flight phases is demonstrated.

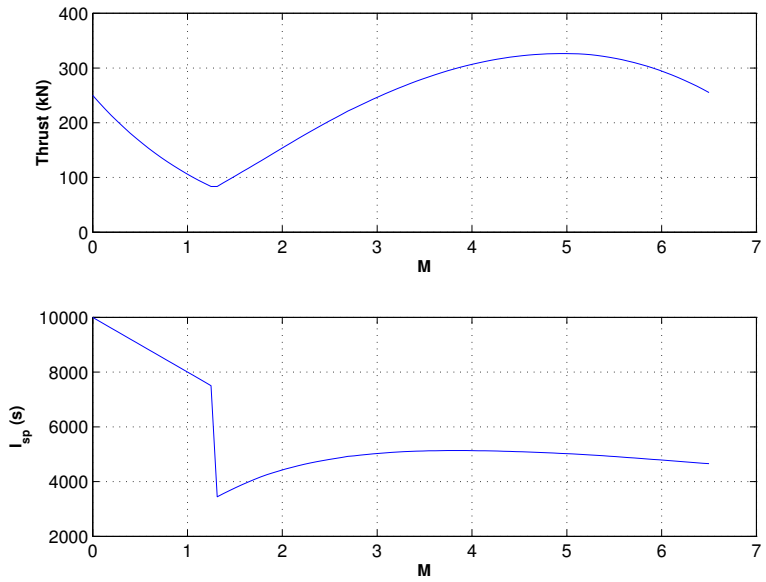

Figure 2: The turbopump and then ramjet produce good performance over the full Mach number range. The altitude varies from 0 to 40 km in the plot.

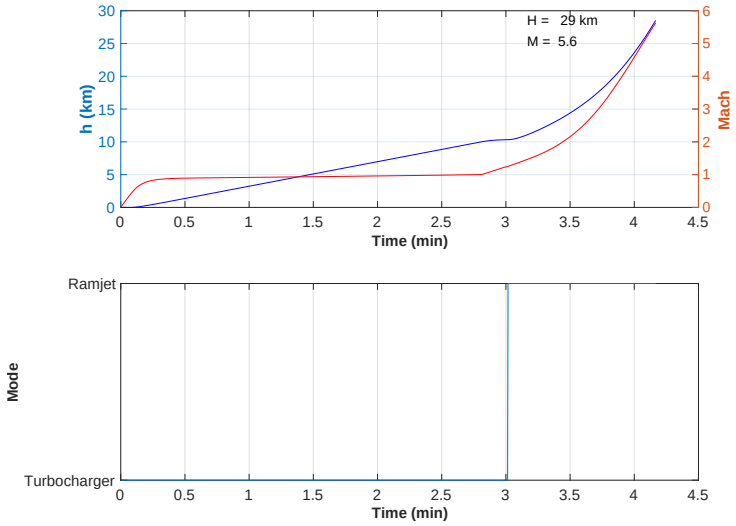

Figure 3: Ascent trajectory with transition at Mach 1.25 at 3 minutes.

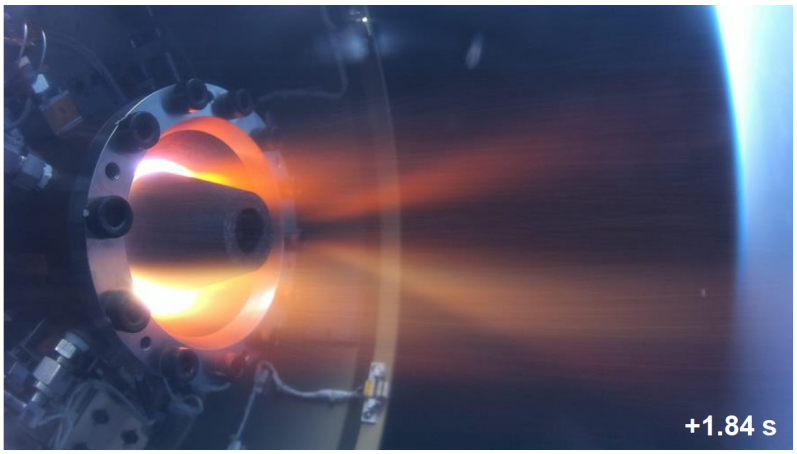

Figure 4: Photo of RDE test in space, where the high-temperature RDE gas plume is shown. Image from Goto et al. (2022) [10].

2. Rotating Detonation Engine

An RDE is an air-breathing aircraft engine that uses a detonation (rather than deflagration) to add energy to the working fluid [14, 15]. Deflagration is the process of heating a material until it burns away. While the flames from deflagration travel at subsonic speeds, the flames from detonation form a shock wave traveling at supersonic speeds. The first detonation sets up a cycle in which the flow circulates the chamber. The pressure from each detonation continues the cycle and forces the exhaust out of the chamber. A compressor is not required but makes the engine more efficient. Unlike a Pulse Detonation Engine, the process is continuous. No chamber purging is required. With detonation, the fuel burns instantaneously, not allowing time for expansion, and this constant volume process can allow higher work output, leading to higher efficiency. A schematic is shown in Figure 5. Annular engines have higher losses than cylindrical engines. However, they are easier to operate. Problems with RDEs include multiple detonations and detonations that cause a reversal of the flow.

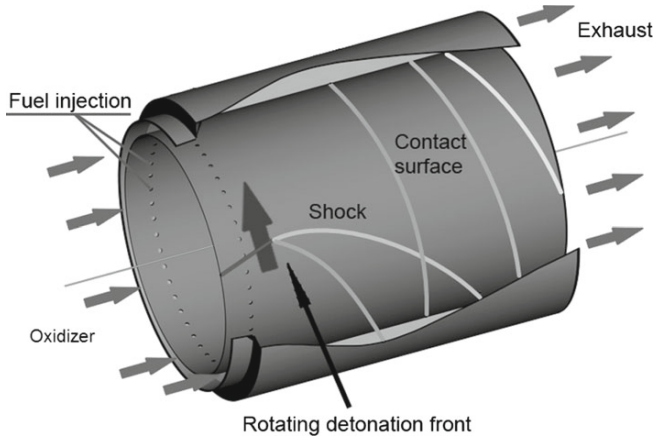

Figure 5: RDE schematic. This is an annular engine [14].

RDEs have historically been plagued by the instability of the detonation wave. Princeton University has added ozone (O_3) to the inlet air. Ozone added from tanks or produced in-situ via plasma can stabilize the detonation. Transition to detonation is observed to occur earlier and more reliably – note 37.5 μs vs. 129 μs [16]. The results show that, with a small amount of ozone addition, the Deflagration to Detonation Time (DDT) time is reduced by up to 77.5%; whereas it only slightly increases the Chapman–Jouguet (detonation wave) velocities by 6.7%.

There may be additional stabilizing mechanisms that could be employed, e.g., applying an axial magnetic field by winding coils around the engine so that the direction of charged particles is biased in the clockwise (or counterclockwise) direction *via* the $\vec{J} \times \vec{B}$ force, where $\vec{J}$ is current density and $\vec{B}$ is the magnetic field.

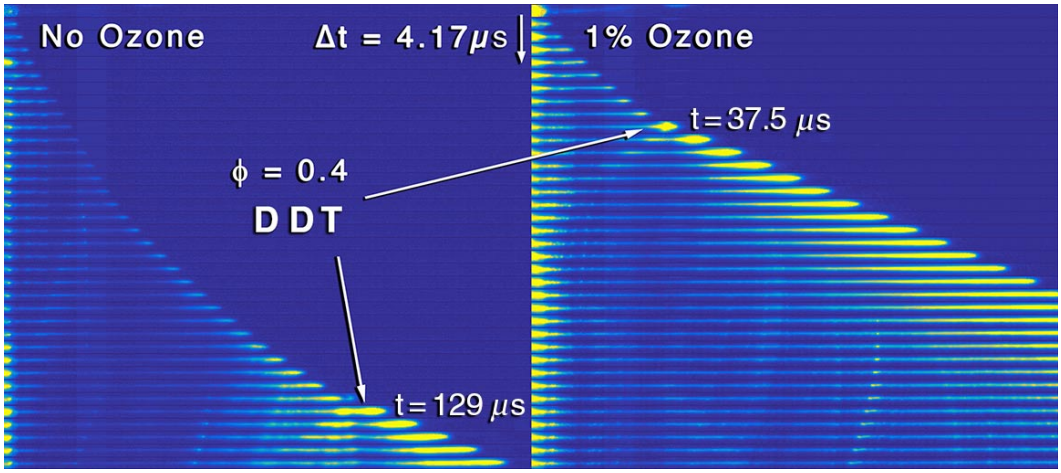

Figure 6: Stacked fast camera images from a detonation wave with (right) and without (left) ozone addition. Image from Sepulveda et al. (2018) [16].

3. ANALYTICAL RDE MODEL

Studies of RDEs generally require computational fluid dynamics. However, for performance studies, analytical models suffice. A MATLAB script is used to model the proposed engine. Assumptions and equations are discussed and sample output across a realistic altitude profile is compared to a typical ramjet. Figure 7 shows the engine and stations.

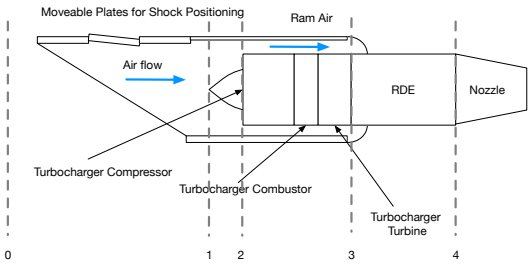

Figure 7: RDE engine concept. It shows the turbocharger at the inlet.

3.1 Background and Assumptions

Ideal Cycle Analysis was used in the development of this model. The inlet, turbopump, RDE, and nozzle assumed isentropic compression and expansion.

Ambient atmospheric conditions were based on standard atmospheric conditions and varied with altitude as per the profile. At the end of this section, plots for a constant altitude profile and space transit mission profile are provided. The flight profile consists of 100 points. For the space transit profile, the first 50 points model a constant climb to 10 km, the following 25 models a cruise at 10 km, and the final 25 represent a rapid climb to 70 km. A constant acceleration in Mach is assumed from 0 on the ground to Mach 8.5 at 70 km.

This model utilizes Chapman-Jouguet (CJ) pressures and temperatures. CJ conditions refer to the pressure and temperature of the rotational detonation wave produced in the ignition chamber of the RDE. The model is based on the Axial Flow Model created by Shepherd and Kasahara [17]. The Axial Flow Model shows the average azimuthal flow around the RDE will be small compared to axial flow speed. Thus, azimuthal flow is neglected in the calculation of specific thrust.

3.2 Model Walkthrough

3.2.1 Atmosphere (Station 0) Station 0 represents atmospheric conditions. Interpolation of the Standard Atmosphere was used to calculate ambient pressure, speed of sound, density, etc. for each point on the altitude profile.

3.2.2 Inlet to Turbopump (Station 2) Station 1 is the inlet and Station 2 is the turbopump intake. Due to the assumption that $\pi_{inlet} = 1$, the stagnation temperatures and pressures at these two stations are equal. The objective of the turbo-pump at low Mach is to pressurize flow enough for combustion in the RDE. This system is similar to a turbocharger in an automobile. Once the ram pressure is sufficient for RDE combustion, the pump is turned off. For operation when the pump is on, Kerrebrock's analysis [18] of a turbojet is carried out by calling the TurbojetNoThrust.m script. Since this ideal cycle analysis is used, a separate normal shock is not applied to station 0 when the turbopump is on.

After the ram pressure transition point, since the airflow is no longer traveling through the turbopump, Mattingly's shock equations [19] are applied to compute static pressure (1) and static temperature (2).

$$P_2 = P_0\Big(\frac{2\gamma}{\gamma+1}M_0^2 - \frac{\gamma-1}{\gamma+1}\Big) \tag{1}$$

$$T_2 = T_0\frac{(\frac{2\gamma}{\gamma-1}M_0^2)(1+\frac{\gamma-1}{2}M_0^2)}{\frac{(\gamma+1)^2}{2(\gamma-1)M_0^2}} \tag{2}$$

3.2.3 Inlet to Combustor (Station 3) The ram pressure transition point is calculated by finding the first instance when the inlet shock stagnation pressure is greater than the turbopump exit stagnation pressure. To compute the stagnation pressure without the turbopump, the free stream pressure ratio from equation (3) is used, and assuming that the pressure ratio across the inlet is 1, equation (4) is used [20].

$$\pi_r = \frac{P_{t0}}{P_0} = \Big(1+\frac{\gamma-1}{2}M_0^2\Big)^{\frac{\gamma}{\gamma-1}} \tag{3}$$

$$P_{3t}^{ram} = \pi_r P_0 \tag{4}$$

The turbopump output stagnation pressure is computed from the output of static pressure from TurbojetNoThrust.m indicated by P_3. To go from static to stagnation, the standard stagnation pressure equation (5) for a specific station is used [20].

$$\frac{P_{3t}^{pump}}{P_3^{pump}} = \left(1 + \frac{\gamma - 1}{2} M^2\right)^{\frac{\gamma}{\gamma - 1}} \tag{5}$$

The transition point occurs at the first instance of $P_{3t}^{ram} > P_{3t}^{pump}$. When the turbopump is off, Mach at the RDE inlet is calculated via a normal shock by AerodynamicShock.m, part of the Princeton Satellite Systems Aircraft Toolbox. Thus, it is assumed that the turbopump contains shocks and its output flow velocity is subsonic. To reiterate, the static pressure and static temperature after the shock when the turbopump is off are calculated via (1) and (2) and the Mach number is calculated using AerodynamicShock.m.

3.2.4 Combustor Exit (Station 4) In the Combustor, CJ velocity is calculated using a process derived by Browne et al. as quoted in Shepherd and Kasahara [17][21]. We use Shepherd and Kasahara's equations of CJ temperature. Explosion Dynamics Laboratory of the California Institute for Technology provided a way to calculate CJ velocity. This model utilizes their Shock and Detonation toolbox [22], a public resource that uses Python and Cantera (.cti) formatted files. The Python toolbox interfaces nicely with MATLAB, and their "Detonation Database" allows the setting of combustion reactants. Below are the reactants used:

$$2H_2 + O_2 + 3.76N_2 \tag{6}$$

CJ velocity values are obtained by inputting the reactants and upstream static temperature and pressure. Shepherd's equation relies on CJ Mach, not velocity, meaning the speed of sound on the detonation wave is required. Because the speed of sound on the detonation wave is dependent on static pressure and static temperature which are dependent on CJ Mach, a speed of sound estimate on the detonation wave is used from calculations done by Shepherd and Kasahara. The estimate indicates CJ Mach is about 2.66 times the speed of sound at station 3.

$$T_{CJ} = T_3 \frac{(\gamma M_{CJ}^2 + 1)^2}{M_{CJ}^2 (\gamma + 1)^2} \tag{7}$$

$$P_{CJ} = P_3 \frac{\gamma M_{CJ}^2 + 1}{\gamma + 1} \tag{8}$$

3.2.5 Calculating Net Thrust and ISP Shepherd and Kasahara provided a net thrust equation (9) derived from the enthalpy of reactants, products, and entropy along the streamline. A full derivation is in their paper [17]. The net thrust equation assumes isentropic expansion along the streamlines and since the specific thrust is mostly independent of exit pressure, CJ conditions can be substituted. Perfect isentropic expansion in the nozzle to ambient pressure is assumed.

$$\left.\frac{\tau}{\dot{M}}\right|_{p0} = a_3 \sqrt{\frac{2}{\gamma - 1}} \left[1 + \frac{1}{2(\gamma + 1)} \left(M_{CJ} - \frac{1}{M_{CJ}}\right)^2 - \left(\frac{P_0}{P_3}\right)^{\frac{\gamma - 1}{\gamma}} \frac{1}{M_{CJ}^2} \left(\frac{\gamma + 1}{\gamma M_{CJ}^2 + 1}\right)^{\frac{-(\gamma + 1)}{\gamma}}\right] \tag{9}$$

Shepherd and Kasahara provide a specific impulse equation (10) derived using the "Pressure History Model", a different approach to modeling RDEs than the Axial Flow Model that uses the average pressure on the thrust wall. The formula is as follows:

$$I_{SPF} = \frac{\tau}{(g Y_f \dot{M})} \tag{10}$$

3.3 RDE Model Results

Here ISP and Specific Thrust are plotted versus flight Mach at a constant altitude of 10000 m. Both the RDE and ramjet were given the same altitude profile.

The following plots (Figure 10 on the next page through Figure 12 on page 8) are based on an altitude profile that represents a space transit mission. The sharp drop and rise in ISP and specific thrust around Mach 7 is caused by the temperature rise that occurs between the Stratosphere and the Mesosphere. In the constant altitude profile, Mach increases linearly from 0 to 8.5. In the space transit profile, Mach increases linearly from 0 to 0.4 for the first half of the flight representing climb, and then increases linearly from 0.4 to 8.5 in the second half of the flight representing acceleration, and then the dash to high altitude.

4. TEST AIRCRAFT DESIGN

4.1 Requirements

The test aircraft is an R/C jet-sized aircraft for testing the RDE engine. This makes the test vehicle very low cost. It allows for manufacturing in a university laboratory.

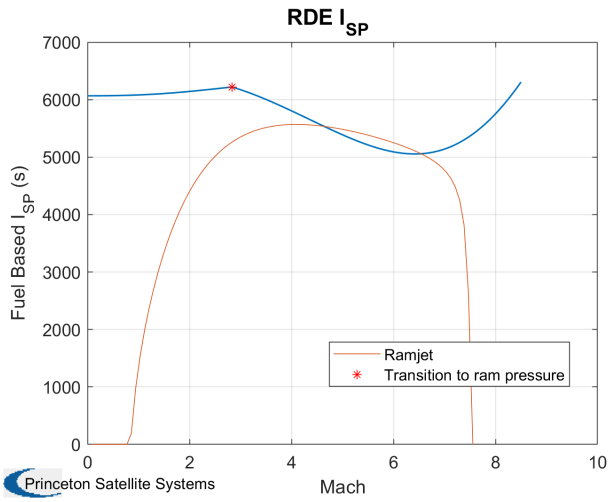

Figure 8: ISP of an RDE compared to a ramjet at 10000 m. The blue line is the RDE.

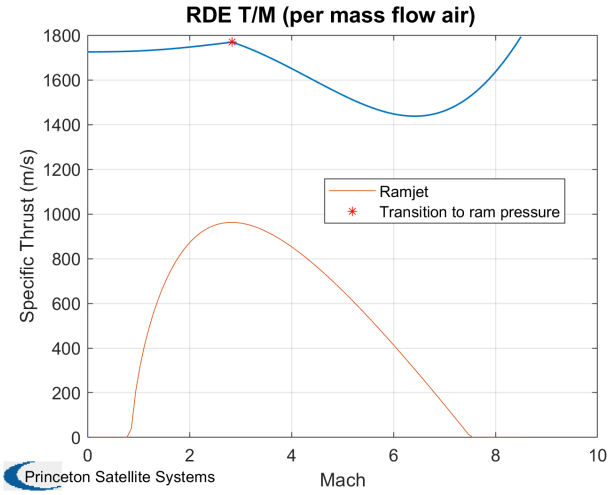

Figure 9: Specific thrust of RDE compared to a ramjet at 10000 m. The blue line is the RDE.

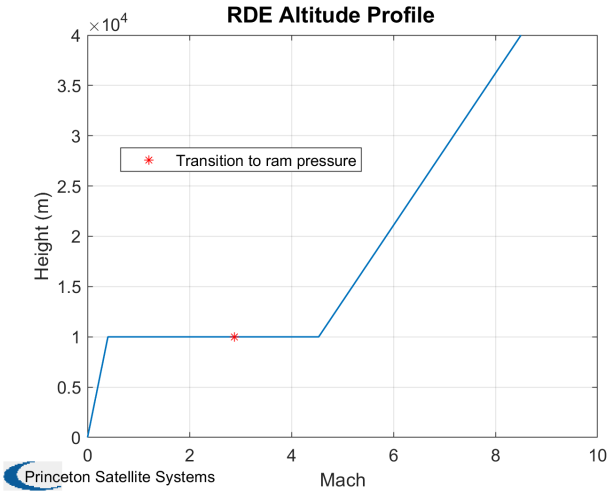

Figure 10: Space Rapid Transit two-stage to orbit altitude profile.

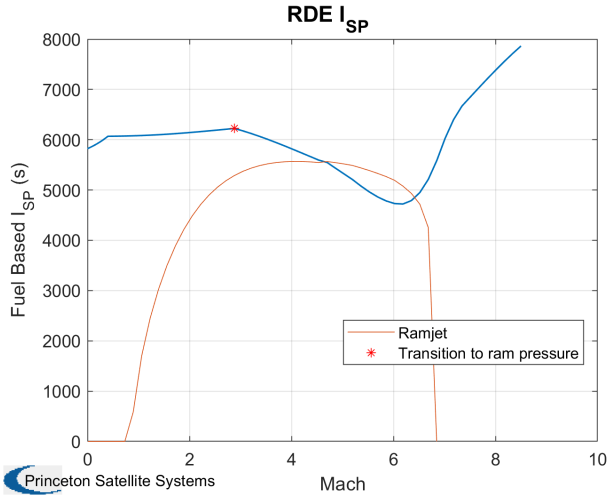

Figure 11: ISP during Space Rapid Transit launch.

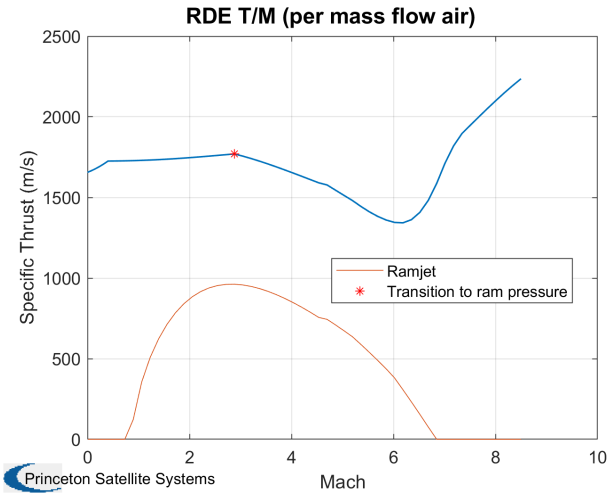

Figure 12: Specific thrust during Space Rapid Transit launch.

4.2 Configuration

The supersonic R/C aircraft employs a delta wing with a single vertical stabilizer. One engine is mounted in the fuselage. The engine would first be tested in an off-the-shelf turbojet R/C engine and then tested in the supersonic R/C aircraft.

4.3 Engine Design

Recent research at Princeton University (PU) has shown that the addition of a small quantity of ozone (O_3) into a combustion tube causes the transition to detonation to occur earlier and more reliably. This alleviates the largest outstanding concern regarding the use of RDEs to power aircraft to high Mach. In an operational system, O_3 would be generated in-situ from atmospheric oxygen using a cold plasma discharge, or O_3 introduced into the airflow from tanks.

RDEs can operate well below the velocity at which ram pressure is sufficient to cause thrust by adding a turbocharger upstream of the RDE to pressurize the inlet air. This allows the RDE to generate thrust even at zero velocity, eliminating the dead weight of a dedicated low-Mach engine. The transition to ram pressure takes place around Mach 2.5. Figure 7 on page 5 shows the concept. The inlet has a turbojet engine configured to produce zero thrust and to just compress the incoming airflow before the RDE combustor. The ram air flows around the turbocharger during ram mode.

Ramjet mode performance is shown in Figure 13 on the facing page. The ram provides the pressure above Mach 1.2.

Using hydrogen as a fuel likewise increases the attractiveness of the RDE system. H_2 contains more than double the specific energy of gasoline, which allows a vehicle with the same fuel ratio as a traditional hydrocarbon-fueled missile to have increased range and velocity. The choice of H_2 also allows the RDE to power the next generation of renewably powered green aircraft, as carbon-neutral propulsion solutions are needed for future aircraft. Hydrogen-fueled aircraft are currently in development [23]. An ATR 72-600 aircraft with a hydrogen retrofit kit [24] was delivered to Jet Blue. Figure 14 shows the

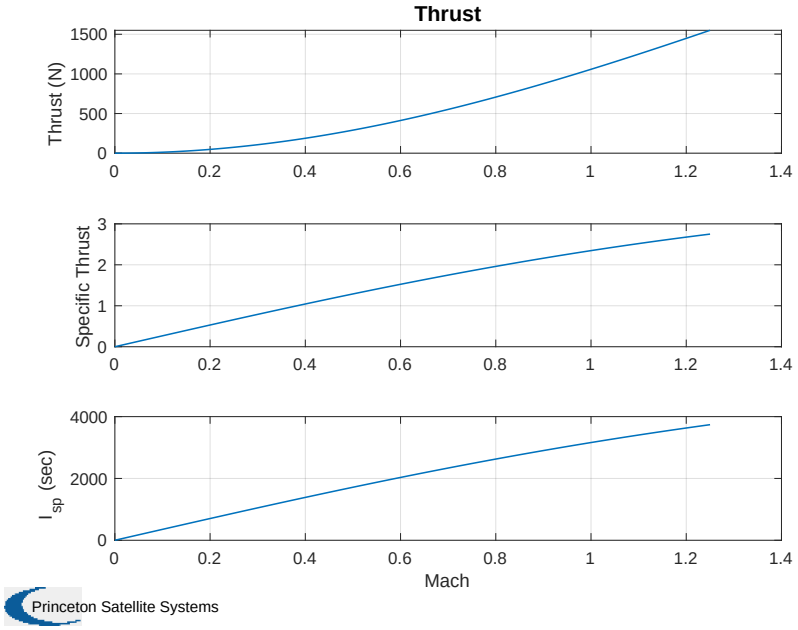

Figure 13: Ideal ramjet performance.

ATR72-600 aircraft next to the retrofit hydrogen tank.

Figure 14: ATR72-600 next to the retrofit tank [24].

The performance of the no-thrust turbocharger is shown in Figure 15.

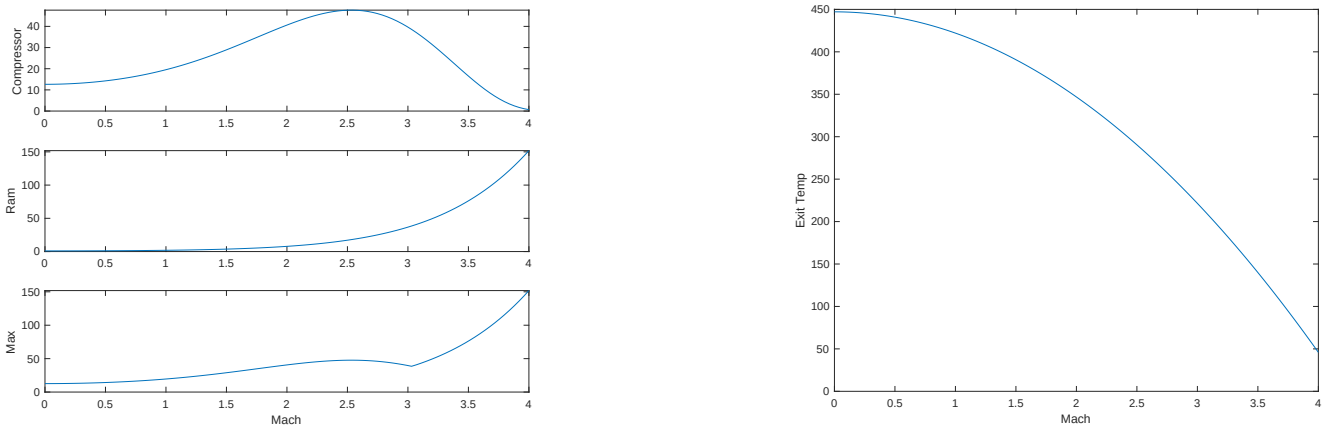

Figure 15: No thrust turbocharger performance. The figures on the left show the pressure ratios with the compressor, ram, and the maximum of the two. The figure on the right shows the exit temperature.

4.4 Aircraft Layout

The aircraft was designed using the Princeton Satellite Systems Aircraft Control Toolbox [25]. A delta-winged aircraft was chosen. The test aircraft will operate up to speeds where the engine can switch from the compressor to ram compression. This allows the test vehicle to test the behavior of the engine during the transition. A notional design is shown in Figure 16 on the next page. The dimensions are in meters. The liquid hydrogen fuel tank is shown above the aircraft.

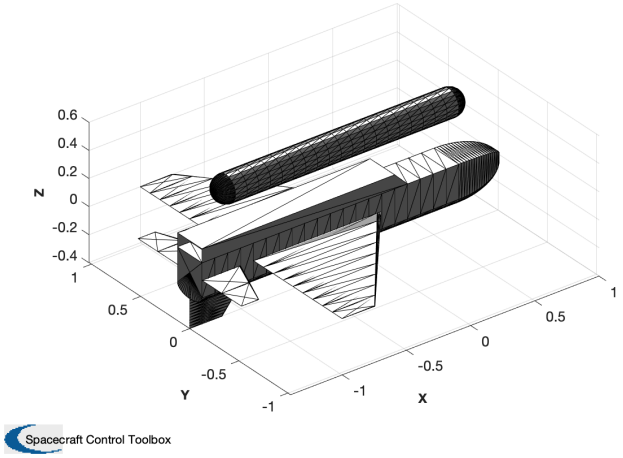

Figure 16: Notional aircraft design. The fuel tank is shown above the aircraft for comparison. The aircraft is roughly two by two meters. The aircraft is similar to the proposed German proposed Hytex aircraft [26].

The design of major subsystems is briefly described in the following sections.

4.4.1 Flight Control The flight control system is implemented using a RaspberryPi MCU.

4.4.2 Wings The wings are a delta planform with vertical and horizontal stabilizers. A single vertical stabilizer is employed.

4.4.3 Fuselage The fuselage contains the fuel tank, discussed below, the battery, receiver, and the other avionics. The engine is mounted below the fuel tank.

4.4.4 Fuel Fuel is H_2 contained in a liquid hydrogen tank. Gloyer-Taylor Laboratories (GTL) has a 2.4-m-long, 1.2-m-diameter cryo tank that has a mass of 12 kg. It holds 150 kg of hydrogen [27]. The fuel tank for the experimental aircraft holds 8 kg of slush hydrogen at 85 kg/m^3 with a diameter of 20 cm and a length of 2.86 m. It does not need insulation or cryo-coolers. Fueling is done just before takeoff. The aircraft would be fueled directly from a liquid hydrogen tanker truck. This is similar to the process for the Boeing Phantom Eye aircraft [28]. Air Products is building an infrastructure for the delivery of hydrogen for truck fleets [28]. Figure 17 shows an Air Products tanker truck and the refueling of the Phantom Eye.

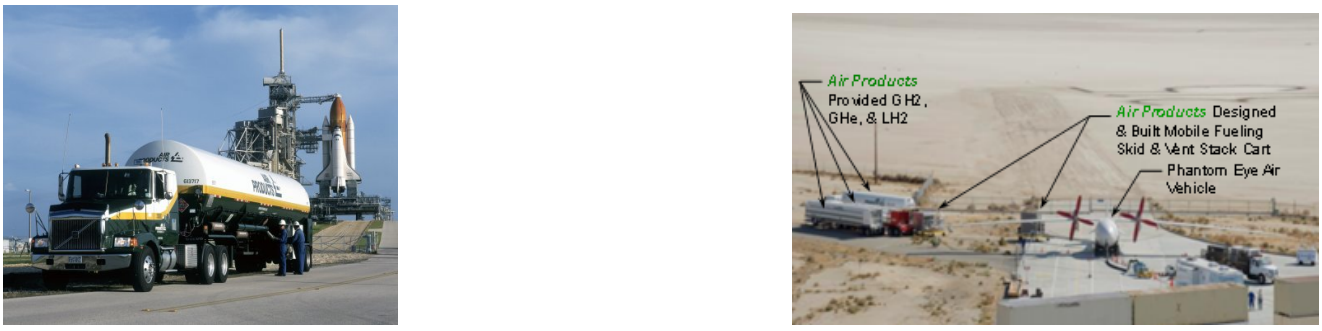

Figure 17: Air Products liquid hydrogen tanker truck and the fueling of the Boeing Phantom Eye liquid hydrogen-fueled aircraft.

Pressurized gaseous tanks are another option. Pressurized hydrogen fuel tanks for vehicles hold compressed hydrogen gas in a range of 3,600 psi – 10,000 psi. Quantum Fuel Systems [29] supplies carbon-fiber reinforced hydrogen fuel tanks.

4.4.5 Aerodynamic Actuators The actuators use linear servo electric actuators. There is the rudder, elevators, and ailerons on each wing.

4.4.6 Power Power is supplied by a lithium battery. All actuators are electric. The power bus delivers power to the actuators, landing gear, and avionics.

4.5 Control System

The overall design of the guidance and control system for the aircraft is illustrated in Figure 18. A pre-computed optimal trajectory provides reference commands for the velocity V_c and flight path angle γ_c over time. The heading command ψ_c is computed based upon the Earth's rotational velocity and the current airspeed V to provide an inertial azimuth angle equal to β, which is the local azimuth angle. The formula for the heading command is:

$$\sin\psi_c = -\left(\frac{V_E}{V}\right)\cos^2\beta + \cos\beta\sqrt{\tan^2\beta - \left(\frac{V_E}{V}\right)^2\sin^2\beta}$$

where $V_E = R_E\omega_E\cos\theta$ is the rotational velocity of the Earth. The formula shows that if we let $V_E \to 0$, the heading command becomes equivalent to the inertial azimuth angle.

Nonlinear dynamic inversion (NDI) is used to track the desired flight path angle and heading angle using the angle of attack α_c and bank angle ϕ_c. The inner loop control tracks the α_c and ϕ_c commands by commanding the control surface deflections, δ_c. The throttle command σ is determined by comparing the current velocity to the reference velocity.

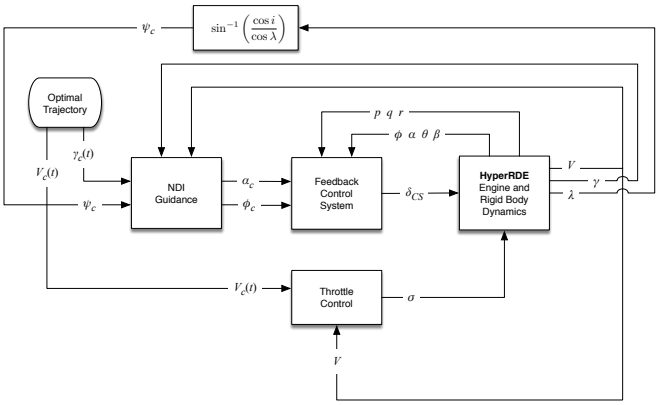

Figure 18: The NDI guidance and control framework. This is a general purpose framework suitable for launch into low-earth orbit.

Using the approach of nonlinear dynamic inversion, we first define desired time-derivatives for flight path angle and heading:

$$\dot{\gamma}_{Des} = K_\gamma\left(\gamma_c - \gamma\right) \tag{11}$$

$$\dot{\psi}_{Des} = K_\psi\left(\psi_c - \psi\right) \tag{12}$$

where K_γ and K_ψ are control gains that may be gain scheduled to provide desired performance across the flight envelope. Also note that the $\dot{\gamma}_{Des}$ command is limited by the maximum allowable normal acceleration, $n_{\max}$, so that:

$$|\dot{\gamma}_{Des}| \leq \frac{n_{\max}}{V}$$

We now derive the required commands for the angle of attack and bank angle by inverting the dynamic equations. The equations of motion for a point mass aircraft model are:

$$\dot{V} = \frac{1}{m}\left(T - \frac{1}{2}\rho(h)V^2SC_D(\alpha)\right) \tag{13}$$

$$\dot{\gamma} = \frac{1}{m}\left(\frac{1}{2}\rho(h)VSC_L(\alpha)\right) - \frac{g\cos\gamma}{V} \tag{14}$$

$$\dot{h} = V\sin\gamma \tag{15}$$

$$\dot{\psi} = \frac{\rho(h)VSC_L(\alpha)\sin\phi}{2m\cos\gamma} \tag{16}$$

Using the angle of attack to track the flight path angle, we have:

$$\alpha_c = C_L^{-1}\left(\frac{2m\left(\dot{\gamma}_{Des} + g\cos\gamma/V\right)}{\rho(h)VS}\right) \tag{17}$$

where C_L^{-1} represents the inverse function of the lift coefficient. The lift coefficient function will need to be modeled as a function of angle of attack, altitude, and Mach number. Using bank angle to track heading, we have:

$$\phi_c = \sin^{-1}\left(\frac{2m\cos\gamma\dot{\psi}_{Des}}{\rho(h)VSC_L(\alpha)}\right) \tag{18}$$

Simulation results from the NDI guidance system are discussed in Section 5.

4.6 Telemetry and Command

The aircraft is designed to operate autonomously during its flight. However, remote piloting is available for all phases of operation.

5. End to End Aircraft Simulations

The test flight was simulated in a point mass simulation. The simulation results are shown in Figure 19 through Figure 24 on page 14. The trajectory is broken into 5 segments:

1. Takeoff roll.
2. Climb at a constant speed to 10 km altitude.
3. Accelerate to the test Mach number of 1.25.
4. Supersonic test period of 8 seconds.
5. Decelerate to the cruise speed of 100 m/s.

The flight parameters are summarized in Table 1 on the facing page. The mission duration is constrained by the amount of hydrogen fuel that can be carried in the aircraft. The fuel tank holds 5 kg of liquid hydrogen. The total fuel consumed by the end of the turn is 3.56 kg.

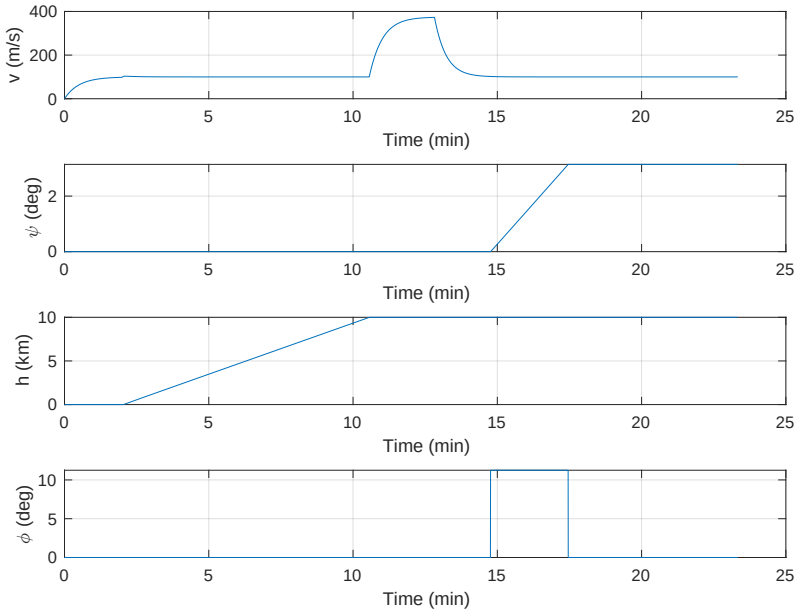

Figure 19: Simulation segment objectives.

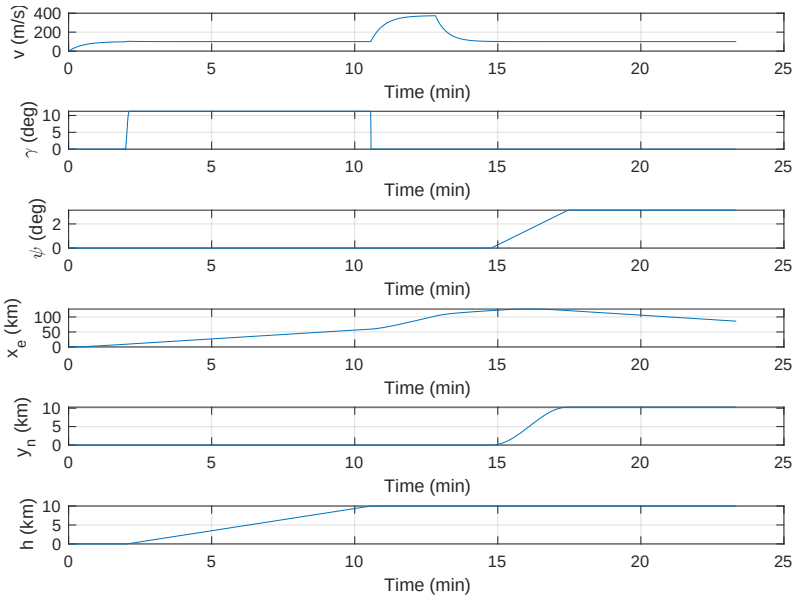

Figure 20: Simulation states.

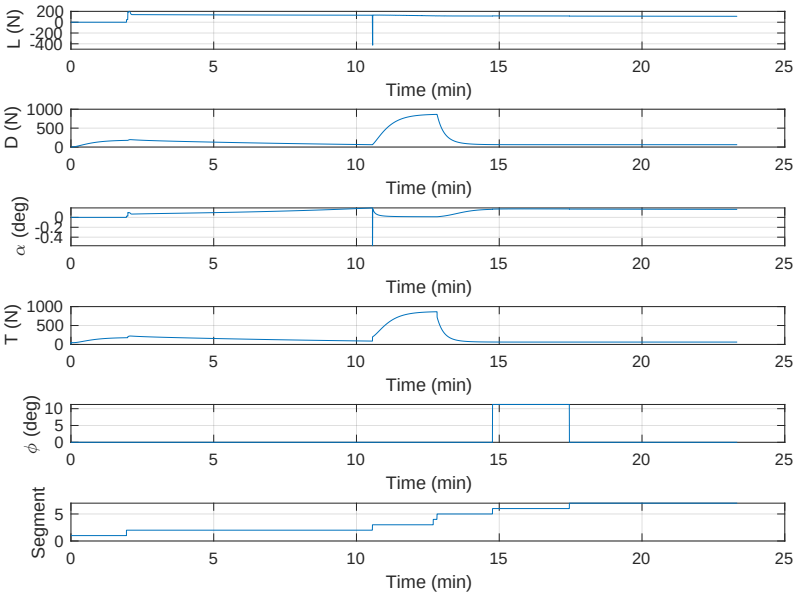

Figure 21: Lift, drag, and thrust. The transient in α is due to the sudden change in flight path angle. γ. This can be fixed by changing it slowly.

Table 1: Flight parameters. Additional time is required to return to the airfield.

Parameter	Value
Duration	23.33 min
Velocity cruise	100.00 m/s
Velocity climb	100.00 m/s
Altitude cruise	10000.00 m
Bank angle	11.25 deg
Climb flight path angle	11.25 deg
Supersonic Test Duration	8.00 s
Test Mach	1.25
Mass Fuel	5.00 kg
Fuel Consumed	3.74 kg
Dry Mass	10.00 kg
Peak Thrust	864.233 N
SFC	0.016 kg/kN/s

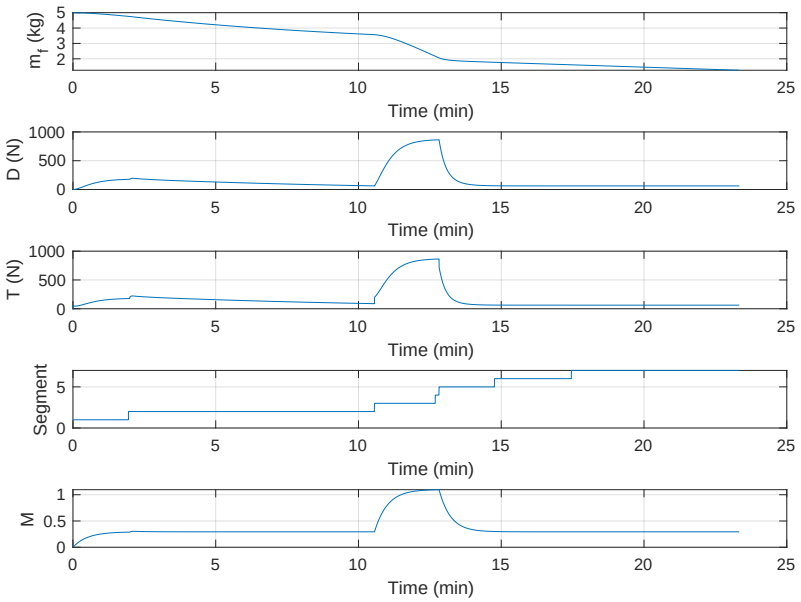

Figure 22: Engine performance. The figure also shows drag.

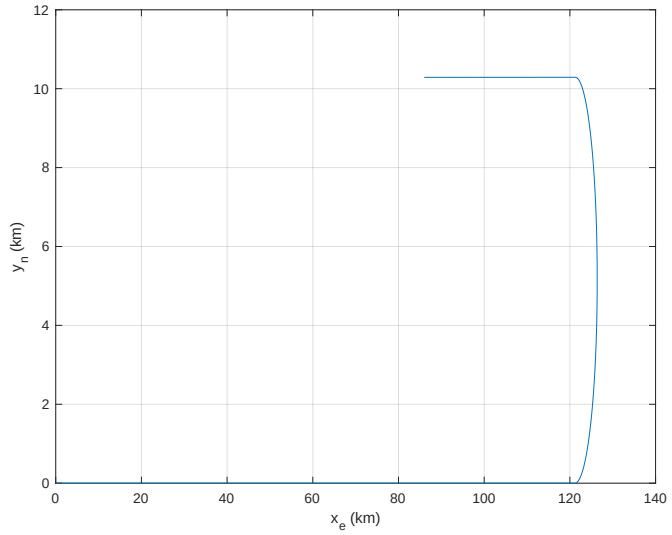

Figure 23: Two-dimensional view of the trajectory.

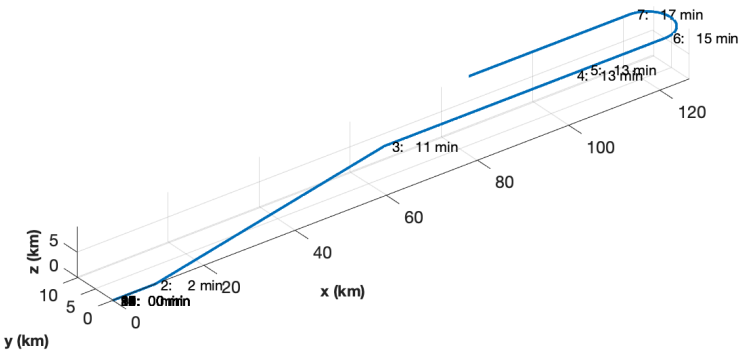

Figure 24: The trajectory with the segments and times numbered.

6. Development Plan

A development plan is proposed. The major steps are:

1. Detailed design of the engine and aircraft
2. Engine testing in a ground test cell
3. Aircraft manufacturing
4. Aircraft flight testing using an R/C gas turbine engine
5. Engine/airframe integration
6. Aircraft flight testing

At the end of this development phase, the RDE engine will have been tested up to the ram pressure transition phase. The flight control will have been verified. The flight data will be used to update the simulations used in this paper to aid the development of an operational version. The RDE combustor will first be tested in an existing R/C aircraft turbine engine. The combustor will replace the existing combustor. This would permit both ground testing and subsonic testing. A commercial off-the-shelf aircraft would be used for the testing.

After that phase, the supersonic R/C aircraft would be built. It would first be tested using the modified R/C engine in subsonic flight. A new engine that would operate up to Mach 2 would then be built. It would be tested in a ground test cell and then in the aircraft.

7. Conclusions

This paper provides an analytical model of an RDE combustor and the design of a small test aircraft to test the performance through ram compression. Results show an improvement in performance over conventional combustors. Even small improvements are important when designing supersonic and hypersonic aircraft and winged launch vehicles. Future work will include testing an RDE combustor in a test cell and testing in the R/C aircraft described in this paper.

References

[1] Mueller, J. B. and Paluszek, M. A., "Space Rapid Transit - A Two Stage to Orbit Fully Reusable Launch Vehicle," *International Astronautical Congress*, No. IAC-14,C4,6.2, October 2014.

[2] Mueller, J. B., Griesemer, P. R., Paluszek, M. A., and Du, J., "Unified GN&C System for the Space Rapid Transit Launch Vehicle," *AIAA GN&C Conference*, August 2010.

[3] Griesemer, P., Mueller, J., Paluszek, M., and Du, J., "System Design of a Reusable, Horizontal Take-Off/Horizontal Landing Two Stage to Orbit Vehicle," *Joint Propulsion Conference*, Nashville, TN, July 2010.

[4] Griesemer, P., Mueller, J., Paluszek, M., and Raghavan, P., "Space Rapid Transit Navigation and Control," *EUCASS 2011*, St. Petersburg Russia, July 2011.

[5] Griesemer, P., Mueller, J., Paluszek, M., and de Castro, E., "Space Rapid Transit for Rapid Spacecraft Deployment," *2011 Reinventing Space Conference*, Los Angeles, California, July 2011.

[6] Flight Global, "Sänger Aerospace Plane Gains Momentum," `http://www.flightglobal.com/pdfarchive/view/1989/1989%20-%202466.html`.

[7] Limited, R. E., "Reaction Engines Limited," http://www.reactionengines.co.uk/index.html.

[8] Kingbury, N., "Aerospace Plane Technology Research and Development in Europe," Tech. Rep. GAO/NSIAD-91-194, GAO, August 1992.

[9] van Pelt, M., *Rocketing into the Future The History and Technology of Rocket Planes*, Springer, 2012.

[10] Goto, K., Matsuoka, K., Matsuyama, K., Kawasaki, A., Watanabe, H., Itouyama, N., Ishihara, K., Buyakofu, V., Noda, T., and Kasahara, J., "Flight Demonstration of Detonation Engine System Using Sounding Rocket S-520-3: Performance of Rotating Detonation Engine," *AIAA SCITECH 2022 Forum*, January 2022.

[11] Institute of Materials and Systems for Sustainability (IMaSS), "World First! Successful Space Flight Demonstration of Detonation Engines for Deep Space Exploration," https://www.imass.nagoya-u.ac.jp/en/research/20210819__kasahara.html.

[12] Law, H., Baxter, T., Ryan, C., and Deiterding, R., "Design and testing of a small-scale laboratory rotating detonation engine running on ethylene-oxygen," *AIAA Propulsion and Energy 2021 Forum*, August 2021.

[13] Anand, V. and Gutmark, E., "Rotating detonation combustors and their similarities to rocket instabilities," *Progress in Energy and Combustion Science*, Vol. 73, 2019, pp. 182–234.

[14] Wolanski, P., "Detonation engines," *Journal of KONES Powertrain and Transport*, Vol. 18, 01 2011, pp. 515–521.

[15] Threewitt, C., "How the Rotating Detonation Engine Works," July 2013.

[16] Sepulveda, J., Rousso, A., Ha, H., Chen, T., Cheng, V., Kong, W., and Ju, Y., "Kinetic Enhancement of Microchannel Detonation Transition by Ozone Addition to Acetylene Mixtures," *AIAA Journal*, 2019.

[17] Shepherd, J. and J., K., "Analytical Models for the Thrust of a Rotating Detonation Engine," September 2017.

[18] Kerrebrock, J., *Aircraft Engines and Gas Turbines*, MIT Press, 1992.

[19] Mattingly, J. D., *Elements of Gas Turbine Propulsion AIAA Education Series*, American Institute of Aeronautics and Astronautics, 2005.

[20] Mattingly, J. D., *Elements of Gas Turbine Propulsion AIAA Education Series*, American Institute of Aeronautics and Astronautics, 2005.

[21] Browne S., J. Z. and Shepherd, J. E., "Numerical Solution Methods for Shock and Detonation Jump Conditions," January 2017.

[22] Shepherd, J. E., "Shock and Detonation Toolbox - 2018 Version," .

[23] Piesing, M., "The epic attempts to power planes with hydrogen," *BBC*, March 2022.

[24] Givens, D., "A JetBlue-Backed Hydrogen-Fuel Powered Airplane Is Coming to the US for Testing," *Robb Report*, July 2022.

[25] PSS, "Aircraft Control Toolbox," https://www.psatellite.com/products/aircraft-control-toolbox/, 2022.

[26] Bulloch, C., "HYTEX - Saenger trailblazer," *Interavia Space Markets*, Vol. 7, No. 3, Jan. 1991, pp. 11–13.

[27] Blain, L., "Ultra-light liquid hydrogen tanks promise to make jet fuel obsolete," April 2022.

[28] AP, "Hydrogen Fueling for Trucks," https://www.airproducts.com/applications/trucks, 2022.

[29] QFS, "Scalable Hydrogen Fuel Systems and Infrastructure," https://www.qtww.com/product/hydrogen/, 2021.